Single-cell heterogeneity in interferon induction potential is heritable and governed by variation in cell state

Elizabeth A. Thayer[1], Gabriela Shipman[1], Joel Rivera-Cardona[1], Tarun Mahajan[2,3], Qi Wen Teo[3,4], J. Sebastian Paez[5], Joseph Lederer[3], Jie Chen[6,7,8], Nicholas C. Wu[3,4,7,9], Sergei Maslov[2,3,9,10], Christopher B. Brooke[1,3]*

[1] Department of Microbiology, University of Illinois Urbana-Champaign, Urbana, IL, USA
[2] Department of Bioengineering, University of Illinois Urbana-Champaign, Urbana, IL, USA
[3] Carl R. Woese Institute for Genomic Biology, University of Illinois Urbana-Champaign, Urbana, IL, USA
[4] Department of Biochemistry, University of Illinois Urbana-Champaign, Urbana, IL, USA
[5] Talus Bioscience, Seattle, WA, USA
[6] Department of Cell and Developmental Biology, University of Illinois Urbana-Champaign, Urbana, IL, USA
[7] Department of Biomedical and Translational Sciences, Carle Illinois College of Medicine, University of Illinois Urbana-Champaign, Urbana, Illinois, USA
[8] Cancer Center at Illinois, University of Illinois Urbana-Champaign, Urbana, IL, USA
[9] Center for Biophysics and Quantitative Biology, University of Illinois Urbana-Champaign, Urbana, Illinois, USA
[10] Center for Artificial Intelligence and Modeling, University of Illinois Urbana-Champaign, Urbana, Illinois, USA
[11] Department of Physics, University of Illinois Urbana-Champaign, Urbana, Illinois, USA
* Corresponding author (cbrooke@illinois.edu)

SUMMARY

Type I and III interferons (IFNs) are among the first lines of defense against viral infections, yet they are generally only produced by a tiny fraction of infected cells. Here, we show that variability in tonic cell signaling significantly influences cells' ability to

32 produce IFN upon stimulation with the synthetic double-stranded RNA,
33 polyinosinic:polycytidylic acid (pIC). Using single-cell approaches, we found that
34 members of the activator protein (AP)-1 transcription factor were implicated in *IFNL1*
35 expression predisposition. This guided us to investigate the role of the mitogen-
36 activated protein kinase (MAPK) pathway, specifically the c-Jun N-terminal kinase
37 (JNK), in *IFNL1* production. We found that inhibition of JNK signaling severely altered
38 the nature of the innate antiviral response upon pIC stimulation, independently of the
39 Janus kinase/signal transducer and activator of transcription (JAK/STAT) pathway.
40 Together, our study emphasizes the influence of intrinsic stochasticity in cell state on
41 heterogeneity in IFN expression.
42
43 **INTRODUCTION**
44 The induction of interferon (IFN) is a critical determinant of infection outcome for a wide
45 variety of viruses[1–5]. Respiratory epithelial cells express both type I and III IFNs (IFNα/β
46 and IFNλ, respectively) as part of their first line of defense against the replication and
47 spread of viruses like influenza A virus (IAV). While most cells in the body can respond
48 to type I IFN, only epithelial cells and a subset of immune cells express the correct
49 receptor for responding to type III IFN[3,6]. Due to this tissue specificity in responsiveness,
50 IFNλ is thought to be less inflammatory while still inducing the expression of IFN-
51 stimulated genes (ISGs) that are important for cellular antiviral defense[1,6].
52
53 Retinoic acid-inducible gene I (RIG-I) and melanoma differentiation-associated protein 5
54 (MDA5) are cytosolic pathogen recognition receptors that recognize viral and synthetic
55 foreign RNAs with distinct molecular features[7–9]. RIG-I and MDA5 share similar
56 downstream signaling pathways, as they activate mitochondrial antiviral-signaling
57 protein (MAVS) and ultimately lead to the nuclear translocation of interferon regulatory
58 factor 3 (IRF3) and the initiation of IFN transcription[6,8]. We and others have
59 demonstrated that only a small percentage of infected cells typically express IFNs,
60 independent of virus type[10–15]. The specific factors contributing to heterogeneity in IFN-
61 induction potential remain poorly understood.
62

63 The existence of substantial phenotypic heterogeneity within cellular populations, even
64 for cells of a given “type”, is a well-established phenomenon. Many studies have
65 investigated how cell-intrinsic factors, such as cell cycle stage, mitogen-activated
66 protein kinase (MAPK) signaling state, and patterns of chromatin accessibility, influence
67 variability in response to a stimulus or other cellular phenotypes[16–21]. Intrinsic 2’-5’-
68 oligoadenylate synthase-like protein (OASL) expression has been recently identified as
69 a critical factor governing cellular heterogeneity in IFN induction potential during IAV
70 infection, but it is not clear whether this effect is IAV-specific[22].
71
72 Here, we investigated the sources of cellular heterogeneity in the ability of A549 cells to
73 produce IFN in response to the commonly used RIG-I agonist, polyinosinic:polycytidylic
74 acid (pIC). We used single-cell RNA sequencing and pseudotime analysis to identify
75 transcriptional determinants of IFN induction potential. Additionally, we found that
76 single-cell clonal populations isolated from a single parental population exhibited
77 massive differences in IFN-induction phenotypes that were maintained over numerous
78 generations. This heritable phenotypic variation correlated in part with basal
79 transcriptional and epigenetic profiles. Using multiple approaches, we identified cellular
80 variation in (a) basal expression of ISGs, and (b) MAPK-activator protein (AP)-1
81 signaling activity as key predictors of the ability of individual cells to mount a robust
82 innate immune response to foreign RNA.
83
84 **RESULTS**

85 **Following pIC treatment, most cells exhibit IRF3 nuclear translocation but do not**
86 **transcribe IFNλ**

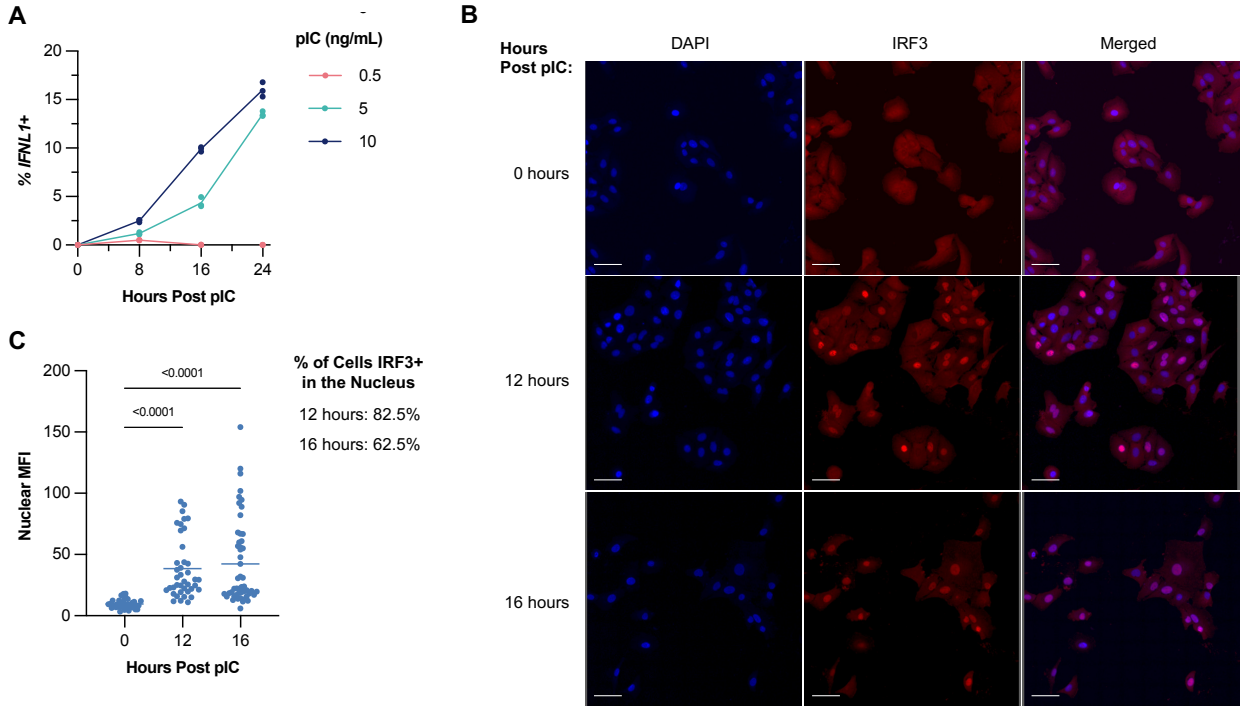

87

88 ***Figure 1. IFNL1 is rarely expressed in A549 cells after pIC stimulation. (A)*** *Percent*
89 *of cells positive for IFNL1 transcripts at 0-, 8-, 16-, and 24-hours post-pIC treatment with*
90 *0.5, 5, and 10 ng/mL concentrations.* ***(B)*** *Representative images of A549 cells*
91 *stimulated with pIC with the nucleus and IRF3 stained. White bars indicate 50 µm.*
92 *Brightness enhanced evenly for publication.* ***(C)*** *Quantification of raw fluorescence of*
93 *IRF3 in the nucleus using Imaris. Significance calculated using Dunnett's multiple*
94 *comparisons. Percent of cells IRF3+ in the nucleus determined by the number of cells in*
95 *the stimulated populations with a higher MFI than the highest untreated cell.*

96

97 Despite the critical importance of the IFN response for host defense, we and others
98 have demonstrated that only a small fraction of cells are generally capable of
99 expressing IFN following viral infection[10–13,23–25]. Viral infection dynamics are highly
100 heterogeneous at the single-cell level, and it is unclear how much of the observed
101 variation in IFN induction is due to cellular heterogeneity in viral processes[14,26,27].

102

103 To examine single-cell heterogeneity in IFN induction without the confounding effects of
104 viral heterogeneity, we treated the human lung adenocarcinoma cell line A549 with
105 increasing concentrations of pIC and quantified *IFNL1* transcription within single cells
106 using hybridization chain reaction[28] fluorescence *in situ* hybridization coupled with flow
107 cytometry (HCR-Flow)[29]. Even after 24 hours post-treatment with the highest dose
108 tested, fewer than 20% of cells expressed detectable levels of *IFNL1* (**Fig. 1A**). Thus,
109 most cells are incapable of expressing IFN in response to pIC, regardless of dosage or
110 timing.
111
112 Activation of pattern recognition receptors like RIG-I or toll-like receptor 3 (TLR3)
113 typically triggers a signaling cascade that results in the phosphorylation and nuclear
114 translocation of IRF3, the primary transcription factor responsible for driving type I and
115 type III IFN induction[6]. If the low frequency of *IFNL1* induction we observed following
116 pIC stimulation was due to a failure to deliver or detect pIC, then we would expect that
117 IRF3 translocation would occur at similarly low frequencies. We treated A549 cells with
118 pIC and measured the percentage of cells in which IRF3 translocated to the nucleus
119 using confocal fluorescent microscopy. We observed IRF3 nuclear translocation in most
120 pIC-treated cells at 12- and 16-hours post-treatment (**Fig. 1B,C**). These results suggest
121 that the low frequency of *IFNL1* induction cannot simply be explained by defects in
122 sensing of pIC or canonical IRF3 signaling.
123

Gene expression profile prior to treatment is predictive of *IFNL1* induction following pIC treatment

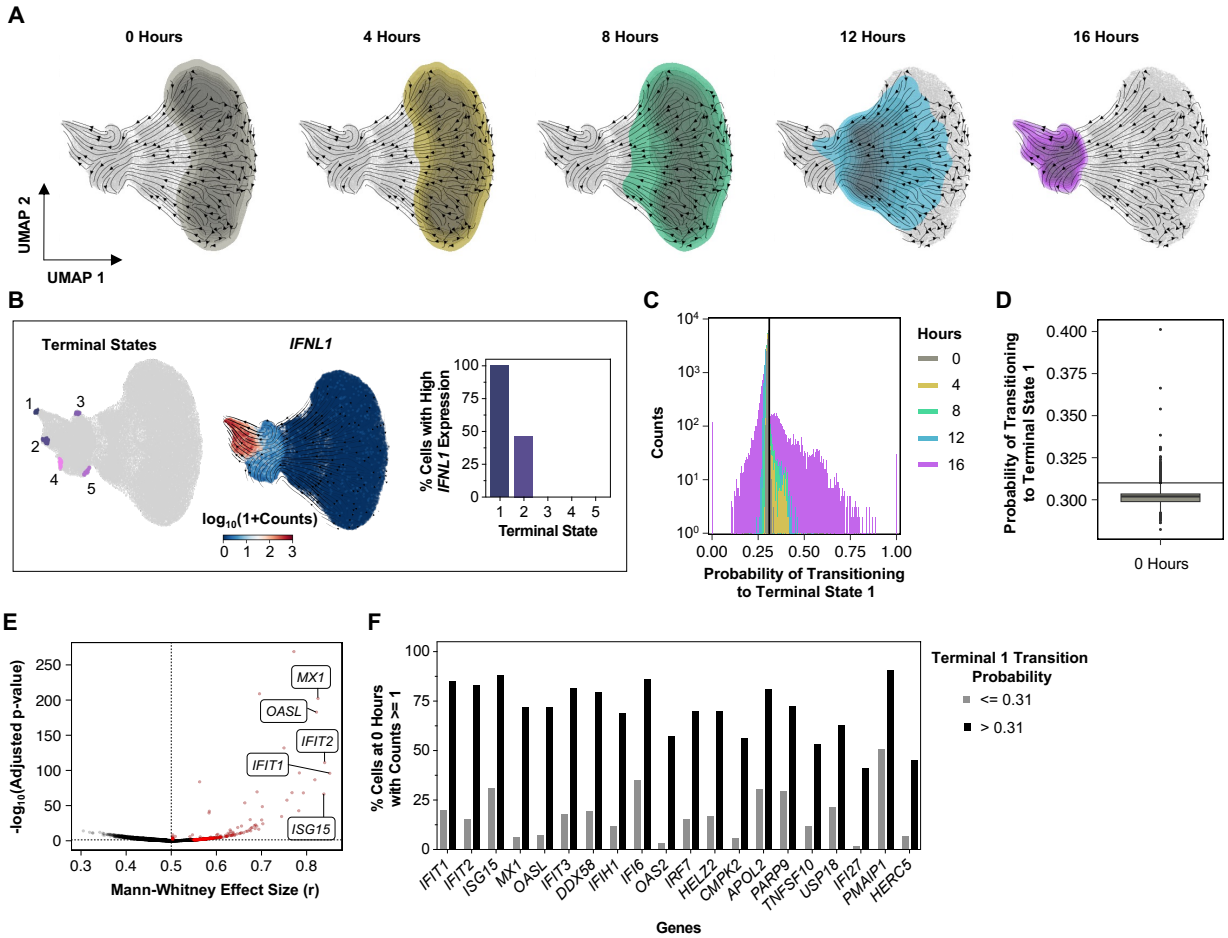

Figure 2. Monitoring the single-cell transcriptional response to pIC using RNA velocity. (A) *UMAP dimensional reduction of the cells from each time point aggregated together, then colored by time point – time indicating sample collection after 5 ng/mL pIC treatment.* ***(B)*** *UMAP dimensional reduction of all cells from every time point. (Left) Terminal states were calculated using temporal-noSpliceVelo and used to determine the probability that each cell in the dataset would end up in those terminal states. (Middle) UMAP dimensional reduction of all cells colored by* $\log_{10}$*(IFNL1 Counts). (Right) Table showing the percent of cells with IFNL1 counts >= 5 within each terminal state (probability = 1).* ***(C)*** *Distribution of the Terminal 1 transition probability of cells in each collection time point. Line at 0.31 indicating the mean transition probability among the full dataset, ultimately being the threshold for high-probability cells.* ***(D)*** *Distribution of the terminal 1 transition probability per cell in the 0-hour collection time point. Line at*

0.31, the previously established as the threshold for high-probability cells. ***(E)*** *Visualization of the genes significantly more expressed in the high-probability cells at 0 hours. Points in black are the unfiltered genes, and points in red are filtered genes - log_{10}(adjusted p-value) > 1.3 and Mann-Whitney effect size > 0.5.* ***(F)*** *Percent of cells at 0 hours expressing the top 20 genes from the Mann-Whitney analysis, separated by the cells' Terminal 1 transition probabilities.*

Pseudotime analysis has previously been used to identify genes whose baseline expression at the single-cell level correlates with the likelihood that a given cell expresses *IFNL1* in response to IAV infection[22,30]. Since active IRF3 signaling alone is insufficient for robust *IFNL1* expression after pIC stimulation, we sought to use this approach to identify other crucial contributors to the *IFNL1* response following pIC treatment. We isolated A549 cells at 0-, 4-, 8-, 12-, and 16-hours post-pIC treatment for single-cell RNA sequencing (scRNA-seq) to then infer the velocity of individual cells moving through the UMAP dimensions (**Fig. 2A**). This approach identified five terminal states at 16 hours, two of which were *IFNL1*+ (**Fig. 2B**).

We next inferred the probability of each individual cell ending up in terminal state 1, the only terminal state where cells were 100% *IFNL1*+ (**Fig. 2B**). The probabilities are not normally distributed and become increasingly bimodal with time, making a correlation analysis between the probabilities and the gene expression of each cell suboptimal. Instead, we set a threshold for high- and low-probability cells, where "high" is classified as having greater than the mean probability across all time points (**Fig. 2C**). This threshold, when plotted on the 0-hour distribution alone, showed that the high-probability cells were outliers, which was consistent with the rarity of *IFNL1*+ cells (**Fig. 2D**). We used the top 4,000 most variable genes across the time points to conduct a Mann-Whitney test to identify genes that are more likely to be expressed in the high-probability cells at 0 hours than the low-probability cells.

This analysis identified 301 genes expressed at the 0-hour time point with an adjusted p-value lower than 0.05 and an effect size greater than 0.5, indicating they are more

likely to be expressed in high-probability cells (**Fig. 2E**). Upon further analysis, we could visualize the result of the test when comparing the percentage of high- or low-probability cells at 0 hours expressing the top 20 genes. All but two of the top genes were expressed in most of the high-probability cells at 0 hours, with all the genes expressed in a greater percentage of high-probability cells (**Fig. 2F**). Additionally, all of the top 20 genes have been reported as ISGs, consistent with the emerging idea that intrinsic ISG expression and/or tonic IFN signaling governs IFN induction potential[22,31].

Single-cell clones exhibit substantial heritable variation in IFN induction potential

Our results indicated that pre-existing heterogeneity within cell populations underlies variability in IFN-induction potential. We next asked whether this variability in IFN-induction potential was transient or if it could be maintained over multiple generations. To distinguish between these possibilities, we sorted single cells from a population of A549 cells and expanded them into 11 individual clonal lines, denoted ET1-ET11.

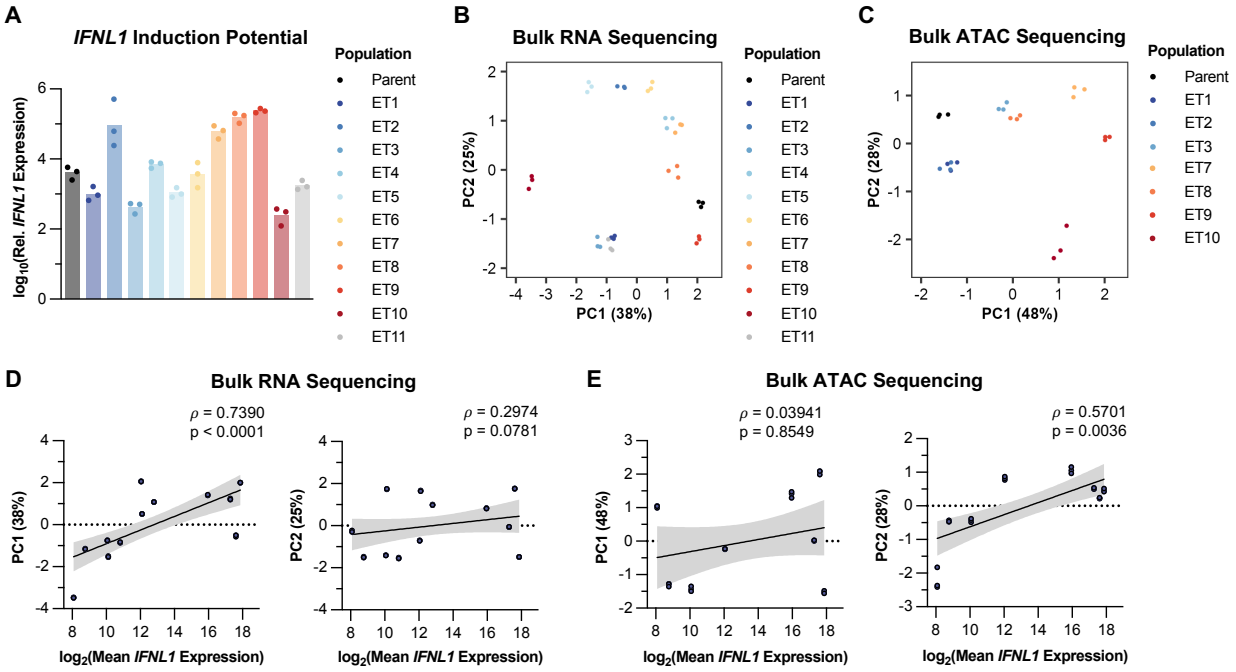

Figure 3. Characterization of clonal cell lines. (A) *IFNL1 expression 16 hours post 0.5 ng/mL pIC treatment among the cell lines was quantified using RT-qPCR. Relative log_{10}(ddCt) fold changes to their ACTB expression and the mean IFNL1 level from the mock of each respective population. One-way ANOVA analysis $p < 0.0001$.* ***(B)*** *PCA plot comparing the transcriptional profiles of each bulk population.* ***(C)*** *PCA plot comparing*

188 *the chromatin accessibility profiles of each bulk population.* ***(D)*** *Correlation between the*
189 *PC1 (left) and PC2 (right) components of the bulk RNA sequencing data and the*
190 *log_2(Mean IFNL1 Expression) of each of the clonal lines. Trendline and 95% confidence*
191 *interval generated with simple linear regression. ρ and p-value calculated based on*
192 *Spearman's correlation.* ***(E)*** *Correlation between the PC1 (left) and PC2 (right)*
193 *components of the bulk ATAC sequencing data and the log_2(Mean IFNL1 Expression) of*
194 *each of the clonal lines. Trendline and 95% confidence interval generated with simple*
195 *linear regression. ρ and p-value calculated based on Spearman's correlation.*
196
197 We treated the parental cell population and the individual clonal lines with 0.5 ng/mL pIC
198 and quantified *IFNL1* induction at 16 hours post-treatment. *IFNL1* transcript levels
199 varied nearly 1000-fold between the individual clonal lines (**Fig. 3A**). Thus, the
200 individual clonal lines exhibited substantial variation in pIC responsiveness that was
201 maintained through the numerous rounds of cell division required to expand them.
202
203 In parallel, we compared the basal transcriptional profiles of the individual clonal lines in
204 the absence of treatment using bulk RNA sequencing and observed that most of the
205 clonal lines diverged substantially from the parental population (**Fig. 3B**). We compared
206 the PC1 component with *IFNL1* induction phenotypes and found a strong correlation
207 between basal transcriptional state and *IFNL1* induction potential (**Fig. 3D**).
208
209 The apparent heritability of heterogeneity in IFN induction phenotypes over numerous
210 generations led us to ask whether this phenotypic variability correlated with any
211 epigenetic signatures. We compared patterns of chromosomal accessibility across the
212 clonal lines using bulk Assay for Transposase-Accessible Chromatin with sequencing
213 (ATAC-seq). We found that global patterns of chromatin accessibility were highly distinct
214 across the clonal lines (**Fig. 3C**). Like what we observed for patterns of transcriptional
215 similarity, ET10 (low *IFNL1* induction) was separated from the group and clearly distinct
216 from ET9 (high *IFNL1* induction). We then asked if variation in the lines' accessibility
217 profiles related to their *IFNL1* responses (**Fig. 3E**). While we did not find a significant
218 correlation between the chromosomal accessibility PC1 and the magnitude of the *IFNL1*

219 response, there was a significant correlation when using the PC2 coordinates (**Fig. 3E**).
220 This suggests that, although the main factor contributing to the heterogeneity in the
221 ATAC data may not be linked to *IFNL1* predisposition, there is significant connection
222 between chromatin accessibility patterns and *IFNL1* expression potential.
223
224 **Variation in basal expression of RIG-I pathway components does not explain the**
225 **heterogeneity in *IFNL1* induction phenotypes**
226 We next sought to determine whether the basal expression patterns of individual
227 transcripts in the clonal populations could also explain heterogeneity in the IFN
228 response to pIC, as we observed in our longitudinal scRNA-seq dataset. We used a
229 generalized linear model, where the x-axis values were the mean $\log_2$ fold changes in
230 *IFNL1* expression of the clonal lines following pIC treatment, and the y-axis values
231 represented the relative expression levels of individual transcripts in the same cell lines
232 in the absence of treatment.
233
234 We first examined the transcripts that encode proteins known to be centrally involved in
235 the RIG-I-based RNA-sensing pathway: *DDX58*, *MAVS*, *TBK1*, and *IRF3*[8,32] (**Fig. 4A,B**).
236 We focused specifically on RIG-I because knocking down other RNA sensors, MDA5
237 (*IFIH1*) and *TLR3*, did not reduce *IFNL1* expression after pIC stimulation as we saw with
238 *DDX58* knockdown, suggesting that the response to pIC in this system is RIG-I-
239 dependent (**Fig. 4A**). While *DDX58, MAVS,* and *TBK1* transcripts did exhibit significant
240 positive correlations with *IFNL1*-induction potential, they only varied in expression levels
241 by 2- to 4-fold across the clonal lines. The expression of the main transcription factor
242 thought to be involved in initiating *IFNL1* expression, *IRF3*, was not significantly
243 correlated with *IFNL1* across the cell lines. Overall, these weak trends appear
244 insufficient to explain the nearly 1000-fold range in IFN expression levels we observed
245 across the clonal lines.

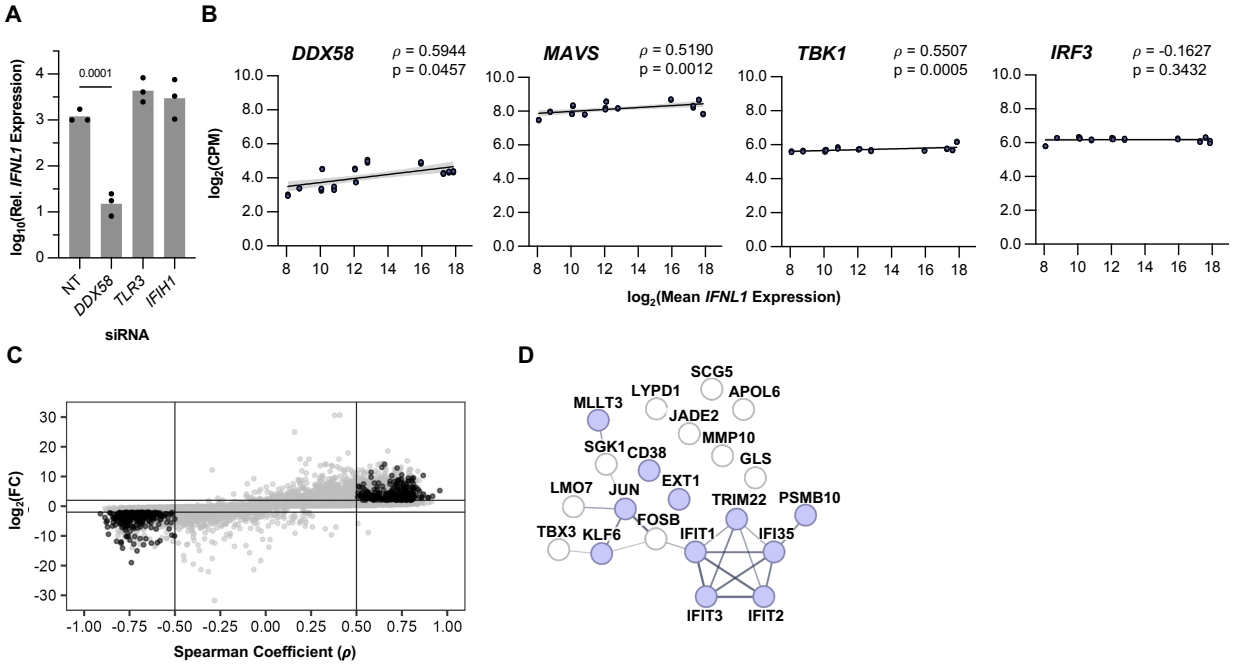

Figure 4. Identification of genes showing a correlation with IFNL1-induction potential. (A) *IFNL1 expression 16 hours post 0.5 ng/mL pIC treatment after 48-hour siRNA treatment was quantified using RT-qPCR. Relative $\log_{10}$(ddCt) fold changes to their ACTB expression and the mean IFNL1 level from the mock of the non-targeting (NT) control. Significance determined by Dunnett's multiple comparisons test.* ***(B)*** *Gene trajectory analysis correlating pIC-induced IFNL1 expression with basal gene expression. Trendline and 95% confidence interval generated with simple linear regression. ρ and p-value generated using Spearman's correlation.* ***(C)*** *Plot of the genes following the generalized linear model (grey), with the genes passing set thresholds of $|\rho| > 0.5$, $-\log_{10}(FDR) > 3$, $|\log_2(FC)| > 2$, and $\log_2(CPM) > 0.1$ (black).* ***(D)*** *STRING analysis of the top genes found in the clonal bulk RNA sequencing and the single-cell data (PPI enrichment $p < 0.0001$). The thickness of the edges indicates the strength of data support for the function and physical protein associations (interaction score > 0.4). Nodes colored purple are annotated to be involved in immune system processes.*

To identify gene products outside of the canonical RIG-I/MAVS pathway that could modulate IFN induction potential, we identified all transcripts that exhibited both (a) a

linear trend (|ρ| > 0.5) between expression level and *IFNL1* induction, and (b) a wide range of expression (|$\log_2$FC| > 2) across the clonal lines (**Fig. 4C**). Over 500 genes passed these filtering criteria, so to narrow down the list we examined the common genes present in both the clone and longitudinal scRNAseq datasets. There were 21 genes in both lists, with significantly more interactions[33] than expected (PPI enrichment $p < 0.0001$), suggesting a significant biological connection (**Fig. 4D**). Indeed, there are known ISGs in the list, *TRIM22*, *IFIT1*, *IFIT3*, *IFIT2*, and *IFI35*[34–36], consistent with the observation that basal ISG expression is associated with enhanced IFN induction potential[22,31]. Notably, two components of the AP-1 complex, *JUN* and *FOSB* were also on this list. While cJun is known to bind to the IFNB enhanceosome[37,38], AP-1 signaling has not been implicated in modulating type III IFN expression. These data raised the possibility of AP-1 signaling as another source of heterogeneity in IFN-induction potential.

MAPK pathway signaling status modulates *IFNL1* induction potential

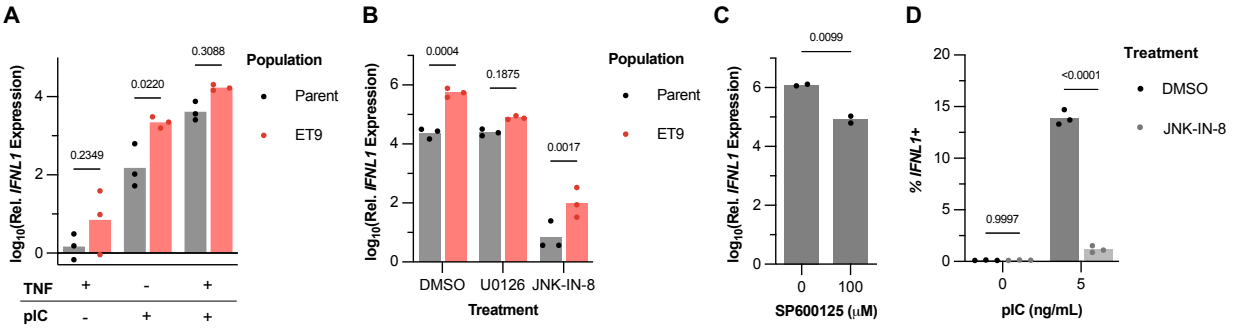

Figure 5. Investigation of pretreatment signaling status involvement in IFN expression. (A) *IFNL1 expression of parental and representative "high" IFNL1 expressor A549 clone in the presence of 10 μM Ruxolitinib with and without 50 ng/mL TNF pretreatment before 0.5 ng/mL pIC treatment for 16 hours. Relative $\log_{10}$(ddCt) fold changes to their ACTB expression and the mean IFNL1 level from the mock of each respective population. Significance determined by Šídák's multiple comparisons test.* ***(B)*** *IFNL1 expression in the parental and representative "high" IFNL1 expressor A549 clone was assessed following pretreatment with 10 μM U0126 or 24 μM JNK-IN-8, followed by 0.5 ng/mL pIC treatment for 16 hours. Relative $\log_{10}$(ddCt) fold changes to their ACTB expression and the mean IFNL1 level from the mock of each respective*

population. Significance determined by Šídák's multiple comparisons test. ***(C)*** *IFNL1 expression of A549 cells after 100 μM SP600125 treatment and subsequent stimulation with 5 ng/mL pIC for 16 hours. Relative log_{10}(ddCt) fold changes to their ACTB expression and the mean IFNL1 level from DMSO without pIC. Significance determined by an unpaired t-test.* ***(D)*** *HCR-Flow measuring the percentage of cells positive for IFNL1 transcripts after DMSO or 24 μM JNK-IN-8 pre-treatment, then 5 ng/mL pIC stimulation for 16 hours. Significance determined by Šídák's multiple comparisons test.*

AP-1 activity is heavily influenced by upstream MAPK signaling and is potently activated by tumor necrosis factor (TNF)[39–42]. To examine the role of AP-1 activity in IFN induction heterogeneity in our system, we first asked how activation of MAPK signaling via TNF pretreatment affected IFN induction by pIC in both the parental A549 cell population and the ET9 clonal line that exhibited a high IFN induction phenotype. However, we wanted to focus only on TNF's potential role in *IFNL1* induction, so we used ruxolitinib[43] pre-treatment to block the JAK/STAT signaling pathway, which is involved in TNF signaling[44]. We found that treatment with TNF alone elicited very little *IFNL1* expression at similar levels in both parental and ET9 populations, indicating that (a) TNF treatment is insufficient to trigger IFN induction in A549 cells, and (b) that TNF responsiveness does not vary significantly across clonal A549 lines, contrasting with pIC responsiveness. Despite TNF not inducing a large amount of *IFNL1* alone, we observed that TNF pre-treatment synergized with pIC stimulation to drive robust *IFNL1* induction in both cell lines, well beyond what would be expected if the contributions of pIC and TNF were simply additive. Importantly, TNF pretreatment reduced variation in IFN induction between parental and ET9 populations, suggesting that variability in IFN induction between clonal lines can be partially overcome by activating the MAPK signaling network (**Fig. 5A**).

We then aimed to inhibit the two MAPKs known to regulate AP-1, JNK and extracellular signal-regulated kinases (ERK), and to examine how this inhibition affected *IFNL1* expression[45,46]. Inhibition of ERK with the MEK inhibitor U0126 did not have a drastic effect on *IFNL1* expression in either population, although it did eliminate the difference

320 between parent and ET9 (**Fig. 5B**). On the other hand, JNK inhibition with the highly
321 selective JNK inhibitor JNK-IN-8[47] almost completely eliminated *IFNL1* expression in the
322 parent and drastically reduced its expression in ET9 (**Fig. 5B**). We also used another
323 JNK inhibitor, SP600125, to affirm our finding with JNK-IN-8. Although it was less
324 dramatic than with JNK-IN-8 treatment, JNK inhibition using SP600125 did lead to a
325 significant decrease in *IFNL1* expression. (**Fig. 5C**). As a follow-up, we wanted to see if
326 this reduction in expression was from the same number of cells producing less *IFNL1*,
327 or if inhibition of JNK signaling changed the number of cells able to produce *IFNL1* in a
328 population. JNK-IN-8 pre-treatment significantly affected the percentage of cells
329 responsive to pIC stimulation (**Fig. 5D**). Together, these data suggest a role for the
330 MAPK/AP-1 signaling network in governing single-cell heterogeneity in IFN induction
331 potential.
332
333 **JNK-IN-8 treatment largely eliminates the transcriptional response to pIC**
334 Given that IFN induction was obliterated by JNK-IN-8 treatment, we next asked whether
335 the entire global transcriptional response to pIC was JNK-IN-8-sensitive. We stimulated
336 A549 cells with pIC in the presence or absence of JNK-IN-8 and the JAK1/JAK2
337 inhibitor ruxolitinib[43] (to block effects downstream of IFN signaling) and quantified
338 transcriptional changes using bulk RNA-seq 16 hours after pIC treatment. As expected,
339 ruxolitinib treatment partially decreased pIC-stimulated *IFNL1* expression in A549s,
340 likely due to the role of IFN signaling in enhancing IFN induction (**Fig. 6A**).
341
342 Treatment with either pIC, JNK-IN-8, or ruxolitinib alone had profound, divergent effects
343 on the cellular transcriptome (**Fig. 6B**). Interestingly, JNK-IN-8 and ruxolitinib pre-
344 treatment shifted the transcriptional phenotype of pIC-treated cells to closely resemble
345 that of the DMSO-only controls. This suggested that almost the entirety of the
346 transcriptional response to pIC in A549 cells could be eliminated by inhibiting both JNK-
347 and JAK-dependent signaling.
348

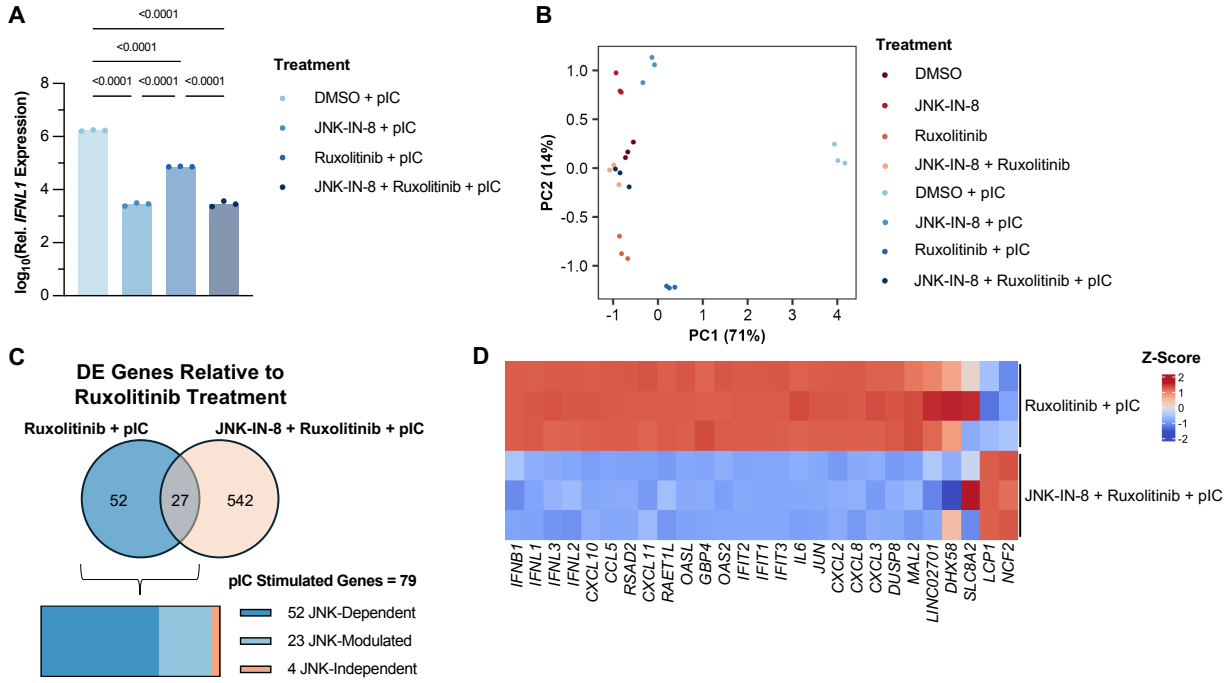

Figure 6. JNK-IN-8 treatment changes the character of the innate immune response. (A) *IFNL1 expression 16 hours post-treatment with 5 ng/mL pIC. Log_{10}(ddCt) relative to ACTB and DMSO-treated control. Inhibitor treatments with 10 μM ruxolitinib and 24 μM JNK-IN-8 4 hours before pIC stimulation. Significance determined by Tukey's multiple comparisons test.* ***(B)*** *PCA plot comparing the transcriptional profiles of the different treatment groups.* ***(C)*** *Venn diagram showing the distinct and shared DE genes in the Ruxolitinib+pIC and JNK-IN-8+Ruxolitinib+pIC treatments. Parts of a whole diagram below detailing what genes of the pIC-stimulated group are JNK-dependent.* ***(D)*** *Heatmap comparing the expression of the shared 27 DE genes of Ruxolitinib+pIC and JNK-IN-8+Ruxolitinib+pIC. Gene expression is relative between the two conditions and is represented by the Z-score.*

To specifically define the JNK-dependent portion of the transcriptional response to pIC, we analyzed the differentially expressed (DE) genes in either the ruxolitinib+pIC or JNK-IN-8+ruxolitinib+pIC group relative to the ruxolitinib-only group (**Fig. 6C**). Fifty-two transcripts were significantly upregulated in the ruxolitinib+pIC group but not in the JNK-IN-8+ruxolitinib+pIC group, likely representing the portion of the transcriptional response to pIC that was fully JNK-dependent. Twenty-seven additional transcripts were DE

367 compared to ruxolitinib-only controls in both groups, but only four appeared unaffected
368 by the presence of JNK-IN-8, suggesting that almost the entirety of the transcriptional
369 response to pIC is fully or partially dependent upon JNK signaling (**Fig. 6D**).
370

371 **DISCUSSION**

372 In this study, we sought to identify the intrinsic sources of cell-to-cell heterogeneity in
373 IFN induction potential observed across a variety of infection systems[10,12–15,22,23,31],
374 using the synthetic dsRNA RIG-I ligand pIC. Using multiple complementary approaches,
375 we identified both basal expression of ISGs and the MAPK/AP-1 signaling network as
376 important determinants of single-cell IFN-induction heterogeneity in this system. While
377 we previously identified a role for intrinsic ISG expression (specifically OASL) in
378 influencing IFN induction potential during IAV infection[22], our data here extend that
379 finding to other stimuli and identify a new role for MAPK/AP-1 signaling in influencing
380 cellular heterogeneity in innate immune function.
381

382 Both our longitudinal scRNAseq experiment and our transcriptional analyses of single-
383 cell-derived clones identified the AP-1 transcription factors *JUN* and *FOSB* as correlates
384 of IFN-induction potential. These factors are activated downstream of the MAPK family,
385 an incredibly complex and highly conserved network of signaling molecules that
386 collectively integrate numerous diverse inputs to regulate multiple aspects of cellular
387 behavior, including innate immune function[48–50]. Because of the large number of input
388 signals that can modulate MAPK activity, including cytokines and various sources of
389 cellular stress, the potential involvement of MAPK/AP-1 signaling opens the door to the
390 possibility of a variety of external and internal stimuli contributing to the tuning of IFN
391 induction potential at the single-cell level.
392

393 To examine the role of the MAPK network and the downstream AP-1 family transcription
394 factors in governing cellular heterogeneity in IFN induction, we took two approaches,
395 each with significant caveats. First, we tried maximizing MAPK signaling activity by
396 pretreating with TNF in the presence of the JAK/STAT inhibitor ruxolitinib. Our findings
397 confirmed previous work demonstrating that TNF can enhance the production of type I

398 IFNs and their downstream ISGs[44,51–53]. Importantly, they also showed that TNF
399 pretreatment reduced the variability in IFN-induction potential between clonal lines of
400 A549 cells. While this is consistent with a role for MAPK signaling in IFN-induction
401 heterogeneity, the effects of TNF stimulation are many (including activation of IRF1[44,52–
402 54]), and thus these results do not provide much clarity on the specific players involved.
403
404 Second, we tried inhibiting AP-1 function by treating with drugs that target the two main
405 pathways connecting MAPK signaling and AP-1: JNK and ERK. Inhibition of JNK
406 activation nearly eliminated bulk expression of *IFNL1* and nearly every other transcript
407 induced by pIC stimulation. JNK-IN-8 treatment also significantly decreased the
408 percentage of cells capable of expressing *IFNL1* after pIC stimulation. In contrast, ERK
409 inhibition had no appreciable effect on IFN induction, suggesting that the effects of
410 MAPK activity on IFN induction are mediated through JNK. While JNK-IN-8 treatment
411 has been reported to exhibit a high degree of specificity for JNK relative to other
412 kinases[45], it is impossible to guarantee specificity at the μM concentrations used here.
413 While we found similar effects on IFN induction with the alternative JNK inhibitor
414 SP600125, we cannot rule out that the effects we observed with JNK inhibitors are due
415 to off-target effects. At a minimum, our results point towards a potential therapeutic role
416 for JNK-IN-8 or other JNK inhibitors in the treatment of some interferonopathies.
417
418 Our finding that cellular heterogeneity in IFN-induction potential could be stably
419 maintained through multiple generations has important implications for understanding
420 innate immune function within epithelial tissues. If there is significant heterogeneity
421 within populations of epithelial stem cells, this heterogeneity could be passed on
422 through transiently amplifying cells into descendant populations of differentiated
423 epithelial cells[55]. This could potentially result in microenvironments with differing
424 sensitivities to innate immune stimuli across the epithelia.
425
426 Though we could not pinpoint a specific mechanism underlying this heritability, it is likely
427 epigenetically encoded. If there were no epigenetic basis for single-cell heterogeneity in
428 pIC responsiveness, we would expect that the numerous generations required to

429 expand individual sorted cells into the clonal lines we examined would eliminate any
430 transient variability in responsiveness seen at the single-cell level. A large body of work
431 has demonstrated that cellular populations can exhibit substantial single-cell
432 heterogeneity in epigenetic states, which gives rise to phenotypic variation[19,21]. These
433 results are also consistent with previous studies demonstrating that IFN expression is
434 subject to epigenetic regulation[20,56–59] and that single cells isolated from populations
435 during CRISPR knockout generation are often not representative of the population as a
436 whole[60,61]. Our results further emphasize the need for extreme caution when interpreting
437 data generated from single-cell clones (*e.g.,* CRISPR knockouts).
438
439 Our results point towards important roles for MAPK/AP-1 signaling and intrinsic ISG
440 expression patterns in determining the fraction of cells capable of responding to viral
441 stimuli by producing IFNs. Because the IFN response is highly non-linear, even small
442 changes in the percentage of IFN-producing cells can have disproportionate effects on
443 the kinetics and magnitude of the downstream antiviral response[62]. The percentage of
444 cells capable of IFN induction effectively sets a threshold of how far viral replication
445 must proceed before triggering an IFN response. Such a system could help avoid
446 unnecessary IFN induction by harmless exposures to PRR ligands, such as might be
447 expected during (a) the limited viral replication that can occur within an immune host, or
448 (b) a transient breakdown in metabolism or containment of host-encoded
449 immunostimulatory RNAs. Future studies should more closely examine how patterns of
450 single-cell heterogeneity in IFN-induction potential vary across different cell populations
451 and environmental contexts.
452
453 **LIMITATIONS OF THE STUDY**
454 There are significant limitations surrounding the use of transformed cell lines like the
455 A549 human lung adenocarcinoma cell line used throughout this study. These cells
456 diverge from primary epithelial cells in many important ways, including genomic stability
457 and immune function. Further work is needed both in primary cell systems and *in vivo* to
458 validate and extend the results we report here. As indicated above, it is impossible to
459 rule out off-target effects when evaluating the results obtained using the JNK inhibitor

drugs. Both our analyses of single-cell clones and our single-cell pseudotime analysis approaches rely upon correlative results, which do not conclude any causal relationship. More work is needed to firmly establish causal relationships.

RESOURCE AVAILABILITY

Lead contact

All additional questions for further information or resources should be directed to the lead contact, Chris Brooke (cbrooke@illinois.edu).

Materials availability

Clonal lines are available upon request.

Data and code availability

All sequencing data can be found at NCBI GEO under accession numbers GSE313066, GSE313067, GSE313068, and GSE313071. The code used for the data analysis in this manuscript can be found at https://github.com/BROOKELAB.

ACKNOWLEDGEMENTS

We thank the scientists at the sequencing facility in the Roy J. Carver Biotechnology Center for their help with consultation and preparation for our many sequencing experiments. We also thank those at HPCBio, specifically Drs. Chris Fields and Jenny Drnevich, for their guidance in navigating downstream data processing and analysis for the sequencing experiments. Additionally, Dr. Kevin Van Bortle was a great source of advice with the ATAC sequencing analysis.

C.B.B was supported by NIH R01 AI139246, NIH R01 AI179910. N.C.W. was funded by NIH R01 AI165475. J.C. was supported by NIH R01 GM089771. S.M. was supported by NSF 2107344.

AUTHOR CONTRIBUTIONS

C.B. and E.A.T. conceptualized the study. E.A.T., G.S., J.R.C., and J.L., performed all the experiments. E.A.T. and J.S.P. conducted all of the bulk RNA and ATAC sequencing data processing and analysis. E.A.T. processed the single-cell RNA sequencing data for

T.M. to perform the temporal-noSpliceVelo analysis, and then E.A.T., with help from J.R.C., analyzed the data further. S.M. and T.M. conceptualized temporal-noSpliceVelo. Q.W.T., J.C., and N.C.W. provided critical reagents. E.A.T. and C.B. wrote the manuscript.

DECLARATION OF INTERESTS

The authors declare the following financial interest: J.S.P. is an employee of Talus Biosciences, Inc., a company developing anticancer therapeutics. All other authors declare no competing interests.

MATERIALS AND METHODS

Cells

Human lung epithelial cells (A549) were a gift from Dr. Jonathan Yewdell and maintained in Gibco's Dulbecco's Modified Eagle's Medium (DMEM) high glucose supplemented with GlutaMax and sodium pyruvate, along with the addition of fetal bovine serum (Avantor) for an ending concentration of 8.3%. The cells were cultured at 37°C with 5% CO_2.

Generation of single cell clonal lines

Low-passage A549 cells were collected for FACS and individual cells were distributed into a 96-well flat-bottom plate (Falcon) containing culture media + 5% Penicillin/Streptomycin (Gibco), with 1 cell per well. The wells were then monitored daily until colonies were visible under a microscope. Each well was tracked for whether it contained only one colony or multiple colonies (indicating that the seeding was not perfectly 1 cell per well). Only wells containing a single colony were trypsinized (0.05% Trypsin-EDTA 1X, Gibco) when confluent and expanded into 24-well plates, then into 6-well plates, and finally into T-25 then T-75 flasks. The clones (ET1-11) were numbered based on the order of initial collection.

Polyinosinic:polycytidylic acid (pIC) treatment

521 A549 cells were transfected using Lipofectamine 3000 (Invitrogen) with the synthetic
522 double-stranded RNA, pIC (Poly(I:C) LMW, InvivoGen), for the indicated time points.
523 After the specified treatment times, the samples were collected based on the specific
524 downstream quantification method.
525
526 **siRNA treatment**
527 We used Dharmacon ON-TARGETplus SMARTpool siRNA (Horizon Discovery) to
528 knock down gene transcripts. The siRNAs used were against human DDX58 (Gene ID:
529 23586, L-012511-00-0005), TLR3 (Gene ID: 7098, L-007745-00-0005), IFIH1 (Gene ID:
530 64135, L-013041-00-0005), and non-targeting control (D-001810-10-05). The A549s
531 were transfected with 30 nM siRNA using Lipofectamine RNAiMAX (Invitrogen)
532 according to the manufacturer's protocol. The cells were incubated for 48 hours, then
533 the RNA was extracted to determine knockdown efficiency, or the cells were treated with
534 pIC as previously described.
535
536 **Tumor necrosis factor (TNF) treatment**
537 JAK1/2 inhibition was achieved using ruxolitinib (MedChemExpress), which was first
538 dissolved in DMSO and diluted to 10 μM in cell culture media. The cells were treated
539 with ruxolitinib for 4 hours before TNF, pIC, or both were added to the cells and
540 remained in the media for the entirety of the incubation. Recombinant human TNF
541 (PeproTech) was diluted to 50 ng/mL in culture media, then added to cells 30 minutes
542 before the cells were either collected for western blot analysis or transfected with pIC.
543 The pIC-transfected cells were incubated for 16 hours, after which the RNA was
544 collected for gene expression analysis.
545
546 **Drug treatments**
547 All inhibitors were dissolved in DMSO and stored at -70°C in single-use aliquots for
548 long-term storage. Each inhibitor was diluted to its working concentration, with the
549 DMSO concentration not exceeding 1%, in culture media and remained in the culture
550 media throughout the experiment. The cells were incubated with the inhibitors for 4
551 hours before the addition of their specified stimulus.

552

553 **RNA isolation, reverse transcription, and gene expression quantification**

554 The cells were first washed with 1X DPBS (Gibco), then lysed with Buffer RLT
555 (QIAGEN). The samples were then collected and processed using the RNeasy Mini Kit
556 (QIAGEN) according to the manufacturer's protocol, or frozen at -70°C until further
557 processing could be performed. cDNA synthesis was performed using the Verso cDNA
558 Synthesis Kit (Thermo Scientific) with the provided anchored oligo(dT) primers,
559 according to the user guide. qPCR could then be performed on the QuantiStudio 3
560 system (Applied Biosystems) with TaqMan reagents (Life Technologies). Gene
561 expression levels were calculated using ΔΔCt, normalizing to ACTB.

562

563 **Western blot analysis**

564 A549 cells were incubated with RIPA lysis buffer supplemented with Halt protease and
565 phosphatase inhibitor cocktail (Thermo Scientific) for 15-30 minutes at 4°C. The lysate
566 was then collected and centrifuged at 20,000xg for 15 minutes. The supernatants were
567 collected, and the protein concentrations were measured using a BCA microplate assay
568 (Thermo Scientific) per the manufacturer's protocol. 10 µg of protein per well was
569 loaded into the Bolt 4-12% Bis-Tris Plus WedgeWell Gel (Invitrogen), then transferred
570 onto a PVDF membrane using the iBlot 2 dry transfer system (Invitrogen).

571

572 The membranes were blocked with StartingBlock blocking solution (Thermo Scientific)
573 and incubated overnight at 4°C. The primary antibodies diluted in blocking buffer used
574 were: Mouse anti-Tubulin (T6792-100UL, Sigma-Aldrich), Rabbit anti-GAPDH (2118S,
575 Cell Signaling Technology (CST)), Mouse anti-Phospho-SAPK/JNK (Thr183/Tyr185)
576 (9255T, CST), Rabbit anti-JNK (10023-1-AP, Proteintech), Mouse anti-p44/42 MAPK
577 (Erk1/2) (4696S), Rabbit anti-Phospho-p44/42 MAPK (Erk1/2) (Thr202/Tyr204) (4370S,
578 CST). After the membranes were incubated, they were washed with DPBS + 0.1%
579 Tween20 (PBST) (Thermo Scientific Chemicals) and incubated with either Goat anti-
580 Rabbit HRP (G-21234, Invitrogen) or Rat anti-Mouse HRP (559751, BD Biosciences) for
581 1 hour at room temperature (RT), then imaged using SuperSignal West Pico PLUS

582 Chemiluminescent substrate (34580, Thermo Scientific) and the iBright 1500 imaging
583 system (Invitrogen).
584
585 **Hybridization chain reaction combined with flow cytometry (HCR-Flow)**
586 HCR-Flow was performed as previously described[29]. As stated, a single cell suspension
587 of A549 cells was prepared by incubating cells with 0.05% Trypsin-EDTA (Gibco) at
588 37°C for 5 minutes. The cell suspension was washed with DPBS (Gibco) and fixed with
589 4% formaldehyde (Thermo Scientific) for 30 minutes at 4°C. After incubation, cells were
590 washed twice with PBST and incubated overnight in 70% ethanol. The single cell
591 suspension was washed twice with PBST and incubated with amplification buffer
592 (Molecular Instruments) for 30 minutes at 37°C. After incubation, 1 μM of each probe
593 (Molecular Instruments) was added to the cell suspension and incubated overnight at
594 37°C. Cells were resuspended in probe wash buffer (Molecular Instruments), incubated
595 at 37°C for 10 minutes, and this was repeated three times. Cells were washed once with
596 5x sodium chloride sodium citrate + 0.1% Tween 20 (SSCT) and incubated in
597 amplification buffer (Molecular Instruments) at RT for 30 mins. After incubation, 3 μM of
598 each snap-cooled hairpin (Molecular Instruments) was added to the cell suspension and
599 incubated at RT overnight. Cells were washed twice with SSCT and analyzed using BD
600 FACSymphony A1.
601
602 **Immunofluorescence microscopy and analysis**
603 A549 cells were transfected with 5 ng/mL pIC and incubated for 16 hours before they
604 were washed with DPBS and fixed with 4% formaldehyde (Thermo Scientific) for 30
605 minutes at 4C. The cells were then washed with PBST three times at RT, permeabilized
606 with DPBS + 0.2% Triton X-100 (Thermo Scientific Chemicals) for 30 minutes, and
607 washed again three times with PBST. Then the cells were blocked with DPBS + 0.1%
608 TritonX-100 + 4% FBS for 30 minutes at RT and incubated with Mouse anti-IRF3
609 (10949S, CST) in the blocking solution for 1 hour at RT. After washing three times with
610 PBST, the cells were incubated with AlexaFluor 647 AffiniPure Donkey anti-Mouse (715-
611 605-150, Jackson ImmunoResearch) in blocking buffer for 1 hour at RT. The cells were
612 washed three times with PBST, stained with DAPI (Thermo Fisher) in PBST buffer for 10

613 minutes at RT, then washed three more times in PBST. Finally, the slides were mounted
614 using ProLong Gold antifade reagent (Invitrogen), and a coverslip was set and sealed
615 with nail polish before imaging on a Zeiss LSM 880.
616
617 The images were analyzed using Imaris (Oxford Instruments). Briefly, DAPI was used to
618 generate 3D objects, and the mean fluorescence intensity (MFI) of the IRF3 signal
619 within the nuclei was recorded. The MFI of untreated versus pIC-treated cells could then
620 be compared to determine the nuclear translocation of IRF3.
621
622 **Bulk RNA sequencing of clonal cell lines**
623 The A549 cell lines ET1-11, along with the parent line, were initially seeded at 1 million
624 cells per well in 6-well plates with three wells per cell line. 24 hours after seeding, the
625 cells were collected, and RNA was isolated as previously described. The Roy J. Carver
626 Biotechnology Center (RJCBC) sequencing facility was responsible for all downstream
627 preparation and sequencing. This included QC, MiSeq (Illumina) titration, cDNA library
628 generation using the TruSeq Stranded mRNAseq Sample Prep kit (Illumina), and
629 sequencing on the NovaSeq 6000 (Illumina) using a S4 flow cell with 2x150nt reads.
630
631 **Bulk RNA sequencing of JNK-IN-8, Ruxolitinib, and pIC-treated A549s**
632 The A549 cells were seeded at 1 million cells per well in 6-well plates, with three wells
633 per condition. Cells were either treated with 1% DMSO, 24 μM JNK-IN-8, 10 μM
634 ruxolitinib, or both inhibitors for 4 hours, then 5 ng/mL pIC was added as previously
635 described. The cells were incubated for 16 hours, then collected for sequencing using
636 the same methods. These samples were also processed and sequenced at the RJCBC
637 sequencing facility. The libraries were prepared with the Kapa Hyper Stranded mRNA
638 library kit (Roche) and sequenced using the NovaSeq X Plus (Illumina) on one 10B lane
639 with 1x100nt reads.
640
641 **Bulk ATAC sequencing of clonal cell lines**
642 The A549 cell lines ET1-11, along with the parent line, were initially seeded at 1 million
643 cells per well in 6-well plates with three wells per cell line. 24 hours after seeding, the

644 cells were trypsinized and collected on ice for transport to the RJCBC for processing.
645 This includes library preparation with the ATACseq kit from Active Motif and sequencing
646 on the NovaSeq X Plus (Illumina) on one 10B lane with 2x150nt reads.
647

648 **Single-cell RNA sequencing of A549s**

649 A549 cells were seeded at 1 million cells per well in 6-well plates. 24 hours after
650 seeding, the cells were treated with 5 ng/mL pIC as previously described. The cells
651 were then collected at their specific time points, transported to the RJCBC on ice, and
652 given to the sequencing facility for further processing and sequencing. The libraries
653 were prepared with the Chromium Next GEM Single Cell Fixed RNA Sample
654 Preparation Kit for Human Transcriptome (10X Genomics) and sequenced using a
655 NovaSeq X Plus (Illumina) on two 10B lanes with 28x150nt reads.
656

657 **Modification and use of temporal-noSpliceVelo for the single-cell RNA**
658 **sequencing dataset**

659 This method of expression-trajectory analysis has been detailed in previous work[22,30].
660 However, we modified the method to address differences in the samples used. Before
661 estimation of fate probabilities, we removed genes associated with the cell cycle
662 to ensure that we could specifically focus on genes that are not directly associated
663 with the cell cycle. For this, we collected cell-cycle genes[63] and filtered them. This led to
664 the removal of 38 genes from the 502 genes that were used to train temporal-
665 noSpliceVelo. We could then use the fate probabilities along with the gene expression
666 profiles of each cell for further analysis, which can be found in our code repository.
667

668 **REFERENCES**

669 1. Galani, I.E., Triantafyllia, V., Eleminiadou, E.-E., Koltsida, O., Stavropoulos, A.,
670 Manioudaki, M., Thanos, D., Doyle, S.E., Kotenko, S.V., Thanopoulou, K., et al.
671 (2017). Interferon-λ Mediates Non-redundant Front-Line Antiviral Protection against
672 Influenza Virus Infection without Compromising Host Fitness. Immunity *46*, 875-
673 890.e6. https://doi.org/10.1016/j.immuni.2017.04.025.

674 2. Sheehan, K.C.F., Lazear, H.M., Diamond, M.S., and Schreiber, R.D. (2015).
675 Selective Blockade of Interferon-α and -β Reveals Their Non-Redundant Functions

676 in a Mouse Model of West Nile Virus Infection. PLOS ONE *10*, e0128636.
677 https://doi.org/10.1371/journal.pone.0128636.

678 3. Piperakis, A., Galani, I.E., and Andreakos, E. (2024). Type III interferons in innate
679 and adaptive immunity in the respiratory tract. Curr. Opin. Immunol. *87*, 102430.
680 https://doi.org/10.1016/j.coi.2024.102430.

681 4. Boehmer, D., and Zanoni, I. (2025). Interferons in health and disease. Cell *188*,
682 4480–4504. https://doi.org/10.1016/j.cell.2025.06.044.

683 5. Duncan, C.J.A., Randall, R.E., and Hambleton, S. (2021). Genetic Lesions of Type I
684 Interferon Signalling in Human Antiviral Immunity. Trends Genet. *37*, 46–58.
685 https://doi.org/10.1016/J.TIG.2020.08.017.

686 6. Lazear, H.M., Schoggins, J.W., and Diamond, M.S. (2019). Shared and Distinct
687 Functions of Type I and Type III Interferons. Immunity *50*, 907–923.
688 https://doi.org/10.1016/j.immuni.2019.03.025.

689 7. Kato, H., Takeuchi, O., Mikamo-Satoh, E., Hirai, R., Kawai, T., Matsushita, K.,
690 Hiiragi, A., Dermody, T.S., Fujita, T., and Akira, S. (2008). Length-dependent
691 recognition of double-stranded ribonucleic acids by retinoic acid–inducible gene-I
692 and melanoma differentiation–associated gene 5. J. Exp. Med. *205*, 1601–1610.
693 https://doi.org/10.1084/jem.20080091.

694 8. Rehwinkel, J., and Gack, M.U. (2020). RIG-I-like receptors: their regulation and roles
695 in RNA sensing. Nat. Rev. Immunol. *20*, 537–551. https://doi.org/10.1038/s41577-
696 020-0288-3.

697 9. Kato, H., Takeuchi, O., Sato, S., Yoneyama, M., Yamamoto, M., Matsui, K.,
698 Uematsu, S., Jung, A., Kawai, T., Ishii, K.J., et al. (2006). Differential roles of MDA5
699 and RIG-I helicases in the recognition of RNA viruses. Nature *441*, 101–105.
700 https://doi.org/10.1038/nature04734.

701 10. Sun, J., Vera, J.C., Drnevich, J., Lin, Y.T., Ke, R., and Brooke, C.B. (2020). Single
702 cell heterogeneity in influenza A virus gene expression shapes the innate antiviral
703 response to infection. PLOS Pathog. *16*, e1008671.
704 https://doi.org/10.1371/journal.ppat.1008671.

705 11. Russell, A.B., Trapnell, C., and Bloom, J.D. (2018). Extreme heterogeneity of
706 influenza virus infection in single cells. eLife *7*. https://doi.org/10.7554/eLife.32303.

707 12. Ramos, I., Smith, G., Ruf-Zamojski, F., Martinez-Romero, C., Fribourg, M., Carbajal,
708 E.A., Hartmann, B.M., Nair, V.D., Marjanovic, N., Monteagudo, P.L., et al. (2019).
709 Innate immune response to influenza virus at single-cell resolution in human
710 epithelial cells revealed paracrine induction of interferon lambda 1. J. Virol.
711 https://doi.org/10.1128/JVI.00559-19.

13. Drayman, N., Patel, P., Vistain, L., and Tay, S. (2019). HSV-1 single-cell analysis reveals the activation of anti-viral and developmental programs in distinct sub-populations. eLife *8*, e46339. https://doi.org/10.7554/eLife.46339.

14. Bruurs, L.J.M., Müller, M., Schipper, J.G., Rabouw, H.H., Boersma, S., Van Kuppeveld, F.J.M., and Tanenbaum, M.E. (2023). Antiviral responses are shaped by heterogeneity in viral replication dynamics. Nat. Microbiol. *8*, 2115–2129. https://doi.org/10.1038/s41564-023-01501-z.

15. Bhushal, S., Wolfsmüller, M., Selvakumar, T.A., Kemper, L., Wirth, D., Hornef, M.W., Hauser, H., and Köster, M. (2017). Cell Polarization and Epigenetic Status Shape the Heterogeneous Response to Type III Interferons in Intestinal Epithelial Cells. Front. Immunol. *8*, 671. https://doi.org/10.3389/fimmu.2017.00671.

16. Wyler, E., Franke, V., Menegatti, J., Kocks, C., Boltengagen, A., Praktiknjo, S., Walch-Rückheim, B., Bosse, J., Rajewsky, N., Grässer, F., et al. (2019). Single-cell RNA-sequencing of herpes simplex virus 1-infected cells connects NRF2 activation to an antiviral program. Nat. Commun. *10*, 4878. https://doi.org/10.1038/s41467-019-12894-z.

17. Preedy, M.K., White, M.R.H., and Tergaonkar, V. (2024). Cellular heterogeneity in TNF/TNFR1 signalling: live cell imaging of cell fate decisions in single cells. Cell Death Dis. *15*, 1–12. https://doi.org/10.1038/s41419-024-06559-z.

18. Goyal, Y., Busch, G.T., Pillai, M., Li, J., Boe, R.H., Grody, E.I., Chelvanambi, M., Dardani, I.P., Emert, B., Bodkin, N., et al. (2023). Diverse clonal fates emerge upon drug treatment of homogeneous cancer cells. Nat. 2023 6207974 *620*, 651–659. https://doi.org/10.1038/s41586-023-06342-8.

19. Carter, B., and Zhao, K. (2020). The epigenetic basis of cellular heterogeneity. Nat. Rev. Genet. 2020 224 *22*, 235–250. https://doi.org/10.1038/s41576-020-00300-0.

20. Yang, J., Tian, B., Sun, H., Garofalo, R.P., and Brasier, A.R. (2017). Epigenetic silencing of IRF1 dysregulates type III interferon responses to respiratory virus infection in epithelial to mesenchymal transition. Nat. Microbiol. 2017 28 *2*, 1–11. https://doi.org/10.1038/nmicrobiol.2017.86.

21. Reffsin, S., Miller, J., Ayyanathan, K., Dunagin, M.C., Heyman, Y., Jain, N., Schultz, D.C., Cherry, S., and Raj, A. (2025). Single-cell susceptibility to viral infection is driven by variable cell states. Cell. https://doi.org/10.1016/j.cell.2025.10.021.

22. Rivera-Cardona, J., Mahajan, T., Kakuturu, N.R., Teo, Q.W., Lederer, J., Thayer, E.A., Rowland, E.F., Heimburger, K., Sun, J., McDonald, C.A., et al. (2025). Intrinsic OASL expression licenses interferon induction during influenza A virus infection. Preprint, https://doi.org/10.1101/2025.03.14.643375.

23. Russell, A.B., Elshina, E., Kowalsky, J.R., Te Velthuis, A.J.W., and Bloom, J.D. (2019). Single-cell virus sequencing of influenza infections that trigger innate immunity. J. Virol. https://doi.org/10.1128/JVI.00500-19.

24. Killip, M.J., Jackson, D., Pérez-Cidoncha, M., Fodor, E., and Randall, R.E. (2017). Single-cell studies of IFN-β promoter activation by wild-type and NS1-defective influenza A viruses. J. Gen. Virol. *98*, 357–363. https://doi.org/10.1099/jgv.0.000687.

25. Zhao, M., Zhang, J., Phatnani, H., Scheu, S., and Maniatis, T. (2012). Stochastic Expression of the Interferon-β Gene. PLoS Biol. *10*, e1001249. https://doi.org/10.1371/journal.pbio.1001249.

26. Schulte, M.B., and Andino, R. (2014). Single-cell analysis uncovers extensive biological noise in poliovirus replication. J. Virol. *88*, 6205–6212. https://doi.org/10.1128/JVI.03539-13.

27. Guo, F., Li, S., Caglar, M.U., Mao, Z., Liu, W., Woodman, A., Arnold, J.J., Wilke, C.O., Huang, T.J., and Cameron, C.E. (2017). Single-Cell Virology: On-Chip Investigation of Viral Infection Dynamics. Cell Rep. *21*, 1692–1704. https://doi.org/10.1016/j.celrep.2017.10.051.

28. Kramer, E.E., Steadman, P.E., Epp, J.R., Frankland, P.W., and Josselyn, S.A. (2018). Assessing Individual Neuronal Activity Across the Intact Brain: Using Hybridization Chain Reaction (HCR) to Detect *Arc* mRNA Localized to the Nucleus in Volumes of Cleared Brain Tissue: Kramer et al. Curr. Protoc. Neurosci. *84*, e49. https://doi.org/10.1002/cpns.49.

29. Rivera-Cardona, J., Kakuturu, N., Rowland, E.F., Teo, Q.W., Thayer, E.A., Tan, T.J.C., Sun, J., Kieffer, C., Wu, N.C., and Brooke, C.B. (2024). Seasonal influenza a virus lineages exhibit divergent abilities to antagonize interferon induction and signaling. PLOS Pathog. *20*, e1012727. https://doi.org/10.1371/journal.ppat.1012727.

30. Mahajan, T., and Maslov, S. (2024). noSpliceVelo infers gene expression dynamics without separating unspliced and spliced transcripts. Preprint, https://doi.org/10.1101/2024.08.08.607261.

31. Pucella, J.N., Maqueda-Alfaro, R.A., Ni, H., Bandeira Sulczewski, F., Eichinger, A., Esteva, E., Ra, A.C., Das, A., Perez, O.A., Feng, J., et al. (2025). Tonic type I interferon signaling optimizes the antiviral function of plasmacytoid dendritic cells. Nat. Immunol. https://doi.org/10.1038/s41590-025-02279-4.

32. Gewaid, H., and Bowie, A.G. (2024). Regulation of type I and type III interferon induction in response to pathogen sensing. Curr. Opin. Immunol. *87*, 102424. https://doi.org/10.1016/j.coi.2024.102424.

33. Szklarczyk, D., Kirsch, R., Koutrouli, M., Nastou, K., Mehryary, F., Hachilif, R., Gable, A.L., Fang, T., Doncheva, N.T., Pyysalo, S., et al. (2023). The STRING

786 database in 2023: protein–protein association networks and functional enrichment
787 analyses for any sequenced genome of interest. Nucleic Acids Res. *51*, D638–
788 D646. https://doi.org/10.1093/nar/gkac1000.

789 34. Schoggins, J.W. (2019). Interferon-Stimulated Genes: What Do They All Do? Annu.
790 Rev. Virol. *6*, 567–584. https://doi.org/10.1146/annurev-virology-092818-015756.

791 35. Yang, H., Winkler, W., and Wu, X. (2021). Interferon Inducer IFI35 Regulates RIG-I-
792 Mediated Innate Antiviral Response through Mutual Antagonism with Influenza Virus
793 Protein NS1. J. Virol. *95*, 10.1128/jvi.00283-21. https://doi.org/10.1128/jvi.00283-21.

794 36. Vicenzi, E., and Poli, G. (2018). The interferon-stimulated gene *TRIM22*: A double-
795 edged sword in HIV-1 infection. Cytokine Growth Factor Rev. *40*, 40–47.
796 https://doi.org/10.1016/j.cytogfr.2018.02.001.

797 37. Maniatis, T., Falvo, J.V., Kim, T.H., Kim, T.K., Lin, C.H., Parekh, B.S., and Wathelet,
798 M.G. (1998). Structure and Function of the Interferon- Enhanceosome. Cold Spring
799 Harb. Symp. Quant. Biol. *63*, 609–620. https://doi.org/10.1101/sqb.1998.63.609.

800 38. Thanos, D., and Maniatis, T. (1995). Virus induction of human IFNβ gene expression
801 requires the assembly of an enhanceosome. Cell *83*, 1091–1100.
802 https://doi.org/10.1016/0092-8674(95)90136-1.

803 39. Karin, M. (1995). The Regulation of AP-1 Activity by Mitogen-activated Protein
804 Kinases. J. Biol. Chem. *270*, 16483–16486.
805 https://doi.org/10.1074/jbc.270.28.16483.

806 40. Aggarwal, B.B., Gupta, S.C., and Kim, J.H. (2012). Historical perspectives on tumor
807 necrosis factor and its superfamily: 25 years later, a golden journey. Blood *119*,
808 651–665. https://doi.org/10.1182/blood-2011-04-325225.

809 41. Westwick, J.K., Weitzel, C., Minden, A., Karin, M., and Brenner, D.A. (1994). Tumor
810 necrosis factor alpha stimulates AP-1 activity through prolonged activation of the c-
811 Jun kinase. J. Biol. Chem. *269*, 26396–26401. https://doi.org/10.1016/S0021-
812 9258(18)47207-9.

813 42. Brenner, D.A., O'Hara, M., Angel, P., Chojkier, M., and Karin, M. (1989). Prolonged
814 activation of jun and collagenase genes by tumour necrosis factor-α. Nature *337*,
815 661–663. https://doi.org/10.1038/337661a0.

816 43. Ostojic, A., Vrhovac, R., and Verstovsek, S. (2011). Ruxolitinib: a new JAK1/2
817 inhibitor that offers promising options for treatment of myelofibrosis. Future Oncol.
818 Lond. Engl. *7*, 1035–1043. https://doi.org/10.2217/fon.11.81.

819 44. Yarilina, A., Park-Min, K.H., Antoniv, T., Hu, X., and Ivashkiv, L.B. (2008). TNF
820 activates an IRF1-dependent autocrine loop leading to sustained expression of
821 chemokines and STAT1-dependent type I interferon–response genes. Nat.
822 Immunol. 2008 94 *9*, 378–387. https://doi.org/10.1038/ni1576.

45. Zhang, T., Inesta-Vaquera, F., Niepel, M., Zhang, J., Ficarro, S.B., MacHleidt, T., Xie, T., Marto, J.A., Kim, N., Sim, T., et al. (2012). Discovery of Potent and Selective Covalent Inhibitors of JNK. Chem. Biol. *19*, 140–154. https://doi.org/10.1016/J.CHEMBIOL.2011.11.010.

46. Favata, M.F., Horiuchi, K.Y., Manos, E.J., Daulerio, A.J., Stradley, D.A., Feeser, W.S., Van Dyk, D.E., Pitts, W.J., Earl, R.A., Hobbs, F., et al. (1998). Identification of a Novel Inhibitor of Mitogen-activated Protein Kinase Kinase*. J. Biol. Chem. *273*, 18623–18632. https://doi.org/10.1074/jbc.273.29.18623.

47. Zhang, T., Inesta-Vaquera, F., Niepel, M., Zhang, J., Ficarro, S.B., Machleidt, T., Xie, T., Marto, J.A., Kim, N., Sim, T., et al. (2012). Discovery of potent and selective covalent inhibitors of JNK. Chem. Biol. *19*, 140–154. https://doi.org/10.1016/j.chembiol.2011.11.010.

48. Peterson, A.F., Ingram, K., Huang, E.J., Parksong, J., McKenney, C., Bever, G.S., and Regot, S. (2022). Systematic analysis of the MAPK signaling network reveals MAP3K-driven control of cell fate. Cell Syst. *13*, 885-894.e4. https://doi.org/10.1016/j.cels.2022.10.003.

49. Wu, C.C.-C., Peterson, A., Zinshteyn, B., Regot, S., and Green, R. (2020). Ribosome Collisions Trigger General Stress Responses to Regulate Cell Fate. Cell *182*, 404-416.e14. https://doi.org/10.1016/j.cell.2020.06.006.

50. Arthur, J.S.C., and Ley, S.C. (2013). Mitogen-activated protein kinases in innate immunity. Nat. Rev. Immunol. *13*, 679–692. https://doi.org/10.1038/nri3495.

51. Wang, W., Xu, L., Brandsma, J.H., Wang, Y., Hakim, M.S., Zhou, X., Yin, Y., Fuhler, G.M., van der Laan, L.J.W., van der Woude, C.J., et al. (2016). Convergent Transcription of Interferon-stimulated Genes by TNF-α and IFN-α Augments Antiviral Activity against HCV and HEV. Sci. Rep. *6*, 25482. https://doi.org/10.1038/srep25482.

52. Veckman, V., Österlund, P., Fagerlund, R., Melén, K., Matikainen, S., and Julkunen, I. (2006). TNF-α and IFN-α enhance influenza-A-virus-induced chemokine gene expression in human A549 lung epithelial cells. Virology *345*, 96–104. https://doi.org/10.1016/j.virol.2005.09.043.

53. Tliba, O., Tliba, S., Da Huang, C., Hoffman, R.K., DeLong, P., Panettieri, R.A., and Amrani, Y. (2003). Tumor Necrosis Factor α Modulates Airway Smooth Muscle Function via the Autocrine Action of Interferon β*. J. Biol. Chem. *278*, 50615–50623. https://doi.org/10.1074/jbc.M303680200.

54. Yamane, D., Feng, H., Rivera-Serrano, E.E., Selitsky, S.R., Hirai-Yuki, A., Das, A., McKnight, K.L., Misumi, I., Hensley, L., Lovell, W., et al. (2019). Basal expression of interferon regulatory factor 1 drives intrinsic hepatocyte resistance to multiple RNA viruses. Nat. Microbiol. 2019 47 *4*, 1096–1104. https://doi.org/10.1038/s41564-019-0425-6.

55. Blanpain, C., Horsley, V., and Fuchs, E. (2007). Epithelial Stem Cells: Turning over New Leaves. Cell *128*, 445–458. https://doi.org/10.1016/j.cell.2007.01.014.

56. Daman, A.W., and Josefowicz, S.Z. (2021). Epigenetic and transcriptional control of interferon-β. J. Exp. Med. *218*, e20210039. https://doi.org/10.1084/jem.20210039.

57. Gao, Z., Li, W., Mao, X., Huang, T., Wang, H., Li, Y., Liu, B., Zhong, J., Renjie, C., Jin, J., et al. (2021). Single-nucleotide methylation specifically represses type I interferon in antiviral innate immunity. J. Exp. Med. *218*, e20201798. https://doi.org/10.1084/jem.20201798.

58. Kamada, R., Yang, W., Zhang, Y., Patel, M.C., Yang, Y., Ouda, R., Dey, A., Wakabayashi, Y., Sakaguchi, K., Fujita, T., et al. (2018). Interferon stimulation creates chromatin marks and establishes transcriptional memory. Proc. Natl. Acad. Sci. *115*, E9162–E9171. https://doi.org/10.1073/pnas.1720930115.

59. Manivasagam, S., Han, J., Teghanemt, A., Keen, H., Sownthirarajan, B., Cheng, B., Singh, A., Lewis, A., Vogel, O.A., Loganathan, G., et al. (2025). Transcriptional repressor Capicua is a gatekeeper of cell-intrinsic interferon responses. Cell Host Microbe *33*, 512-528.e7. https://doi.org/10.1016/j.chom.2025.02.017.

60. Panda, A., Suvakov, M., Mariani, J., Drucker, K.L., Park, Y., Jang, Y., Kollmeyer, T.M., Sarkar, G., Bae, T., Kim, J.J., et al. (2023). Clonally Selected Lines After CRISPR-Cas Editing Are Not Isogenic. CRISPR J. *6*, 176–182. https://doi.org/10.1089/crispr.2022.0050.

61. Bradley, H., Barr, J.N., and Stacey, M. (2024). Single cell variation and rapid emergence of phenotypic heterogeneity in cell lines- a cautionary tale for devotees of CRISPR-Cas9. Preprint at bioRxiv, https://doi.org/10.1101/2024.09.27.615490.

62. Callard, R., George, A.J.T., and Stark, J. (1999). Cytokines, Chaos, and Complexity. Immunity *11*, 507–513. https://doi.org/10.1016/S1074-7613(00)80125-9.

63. Viner-Breuer, R., Yilmaz, A., Benvenisty, N., and Goldberg, M. (2019). The essentiality landscape of cell cycle related genes in human pluripotent and cancer cells. Cell Div. *14*, 15. https://doi.org/10.1186/s13008-019-0058-4.